EPR and FTIR Analysis of the Mechanism of H−2 Activation by [FeFe]−Hydrogenase HydA1 from Chlamydomonas reinhardtii

ARTICLE *in* JOURNAL OF THE AMERICAN CHEMICAL SOCIETY · APRIL 2013

Impact Factor: 12.11 · DOI: 10.1021/ja4000257 · Source: PubMed

8 AUTHORS, INCLUDING:

David Mulder
National Renewable Energy Laboratory
22 PUBLICATIONS **448** CITATIONS
SEE PROFILE

Amanda S Byer
Montana State University
29 PUBLICATIONS **332** CITATIONS
SEE PROFILE

Joan B. Broderick
Montana State University
88 PUBLICATIONS **2,999** CITATIONS
SEE PROFILE

Paul W King
National Renewable Energy Laboratory
58 PUBLICATIONS **2,085** CITATIONS
SEE PROFILE

JACS
JOURNAL OF THE AMERICAN CHEMICAL SOCIETY
Article
pubs.acs.org/JACS

EPR and FTIR Analysis of the Mechanism of H_2 Activation by [FeFe]-Hydrogenase HydA1 from *Chlamydomonas reinhardtii*

David W. Mulder,[†] Michael W. Ratzloff,[†] Eric M. Shepard,[‡] Amanda S. Byer,[‡] Seth M. Noone,[†] John W. Peters,[‡] Joan B. Broderick,[‡] and Paul W. King*[,†]

[†]Biosciences Center, National Renewable Energy Laboratory, Golden, Colorado 80401, United States
[‡]Department of Chemistry and Biochemistry, Montana State University, Bozeman, Montana 59717, United States

Supporting Information

ABSTRACT: While a general model of H_2 activation has been proposed for [FeFe]-hydrogenases, the structural and biophysical properties of the intermediates of the H-cluster catalytic site have not yet been discretely defined. Electron paramagnetic resonance (EPR) spectroscopy and Fourier transform infrared (FTIR) spectroscopy were used to characterize the H-cluster catalytic site, a $[4Fe\text{-}4S]_H$ subcluster linked by a cysteine thiolate to an organometallic diiron subsite with CO, CN, and dithiolate ligands, in [FeFe]-hydrogenase HydA1 from *Chlamydomonas reinhardtii* (CrHydA1). Oxidized CrHydA1 displayed a rhombic 2.1 EPR signal (g = 2.100, 2.039, 1.997) and an FTIR spectrum previously assigned to the oxidized H-cluster (H_{ox}). Reduction of the H_{ox} sample with 100% H_2 or sodium dithionite (NaDT) nearly eliminated the 2.1 signal, which coincided with appearance of a broad 2.3−2.07 signal (g = 2.3−2.07, 1.863) and/or a rhombic 2.08 signal (g = 2.077, 1.935, 1.880). Both signals displayed relaxation properties similar to those of [4Fe-4S] clusters and are consistent with an $S = {}^1/_2$ H-cluster containing a $[4Fe\text{-}4S]_H^+$ subcluster. These EPR signals were correlated with differences in the CO and CN ligand modes in the FTIR spectra of H_2- and NaDT-reduced samples compared with H_{ox}. The results indicate that reduction of $[4Fe\text{-}4S]_H$ from the 2+ state to the 1+ state occurs during both catalytic H_2 activation and proton reduction and is accompanied by structural rearrangements of the diiron subsite CO/CN ligand field. Changes in the $[4Fe\text{-}4S]_H$ oxidation state occur in electron exchange with the diiron subsite during catalysis and mediate electron transfer with either external carriers or accessory FeS clusters.

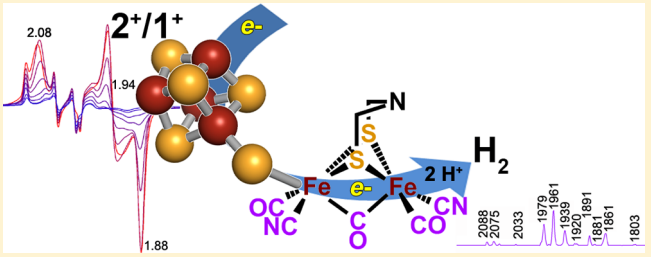

INTRODUCTION

[FeFe]-hydrogenases catalyze the activation of molecular H_2 through the reversible reaction $H_2 \rightleftarrows 2H^+ + 2e^-$. Physiologically, they can function to couple H_2 oxidation to energy-yielding processes, to evolve H_2 at high turnover rates as a means to dispose of reducing equivalents that accumulate during fermentation, or in the case of green algae to couple the reducing potential generated by photosynthetic water oxidation to the evolution of H_2.[1,2] Developing a fundamental understanding of the mechanisms by which enzymes activate small molecules and catalyze fuel-forming reactions may lead to efficient synthetic catalysts for the development of renewable energy solutions for the future.

For [FeFe]-hydrogenases, the activation of H_2 occurs at the H-cluster, which has been structurally characterized by X-ray crystallography.[3,4] The H-cluster is composed of a [4Fe-4S] subcluster ($[4Fe\text{-}4S]_H$) coupled by a protein-derived cysteine thiolate ligand to a diiron subsite ($2Fe_H$) that is additionally coordinated by non-protein CO, CN, and dithiolate ligands (Figure 1). The CO and CN ligands, which were initially identified by Fourier transform infrared (FTIR) spectroscopy,[6,7] help establish the proper balance between σ-donation and π-back-donation required for reversible H_2 binding and heterolytic cleavage of the H−H bond.[8] In particular, CO ligands are strong electron-withdrawing ligands and are critical for reducing back-donation to H_2, preventing dihydride formation while increasing the electrophilicity of the $2Fe_H$ subsite.[8] In addition to helping maintain a low-spin state of the $2Fe_H$ subsite, the CN ligands potentially serve to tune the frontier orbitals of the $[4Fe\text{-}4S]_H$ cubane and $2Fe_H$ subsite to facilitate electron transfer (ET) between the subclusters.[9]

A general model[10] for H_2 activation by the H-cluster based on the interconversion between two redox intermediates, H_{ox} and H_{red}, has been developed (Figure 1). The mechanism was primarily derived from experimental data on a subset of [FeFe]-hydrogenases that can be described as mixed FeS cluster systems. These enzymes, such as *Clostridium pasteurianum* (CpI and CpII), *Desulfovibrio desulfuricans* (DdH), and *Desulfovibrio vulgaris* Hildenborough (DvH), contain, in addition to the H-cluster, accessory FeS clusters ([2Fe-2S] and/or [4Fe-4S], termed F-clusters) that function in ET between the H-cluster and external redox partners. Extensive electron paramagnetic resonance (EPR) studies[11−16] on these enzymes revealed a

Received: January 2, 2013

   dx.doi.org/10.1021/ja4000257 | J. Am. Chem. Soc. XXXX, XXX, XXX−XXX

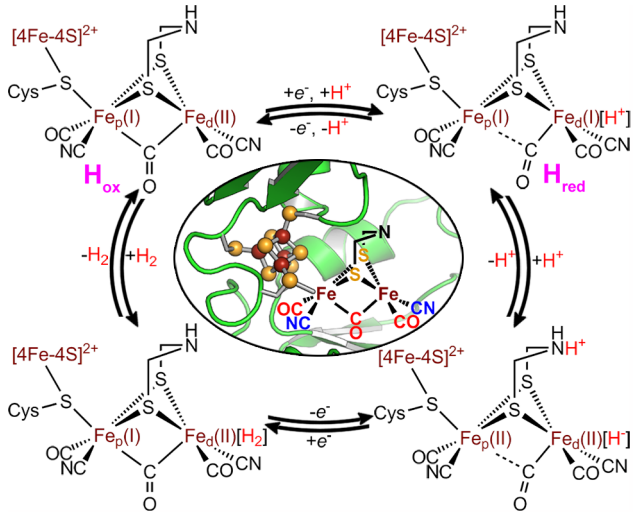

Figure 1. Schematic illustrations of the H-cluster catalytic site present in oxidized [FeFe]-hydrogenase CpI (center) and the general reaction cycle for H_2 catalysis (periphery).[10] Protein secondary structure coordinates were taken from PDB entry 3C8Y, and the dithiolate ligand of the H-cluster is depicted as an azadithiolate.[5,17]

distinctive rhombic 2.1 EPR signal in H_{ox} that has been assigned to an H-cluster having a $[4Fe\text{-}4S]_H^{2+}$ subcluster and a paramagnetic mixed-valent [Fe(I), Fe(II)] $2Fe_H$ subsite. Reduction of H_{ox} to H_{red} leads to an EPR signal assigned to F-clusters and a diamagnetic H-cluster. The H_{ox} and H_{red} intermediates (Figure 1) have unique IR signatures that reflect small structural rearrangements of the CO/CN ligand field.[6,7,17−19] Other catalytic intermediates of H_2 activation and proton reduction by the H-cluster have been only partially characterized because of the complexity of the systems under investigation.

Studies of H-cluster synthetic models have circumvented the complexity of mixed FeS cluster systems, enabling the characterization of different catalytic intermediates involving various CO/CN ligand arrangements and hydride intermediates.[20,21] One particular study on an H-cluster mimic incorporating a $2Fe_H$ subsite linked to a [4Fe-4S] cluster gives precedent for the formation of a $[4Fe\text{-}4S]_H^{+}$ subcluster during catalysis.[22] This contrasts with the mechanistic model shown in Figure 1, which proposes that the $[4Fe\text{-}4S]_H$ subcluster essentially remains in the 2+ oxidation state while the $2Fe_H$ subsite cycles through $S = {}^1/_2$ and diamagnetic states.[23,24] While the significance of this inconsistency is unclear, it provides a basis for additional spectroscopic studies on the nature of H-cluster intermediates during H_2 catalysis.

Recently, HydA1 from *Chlamydomonas reinhardtii* (CrHydA1), a minimal [FeFe]-hydrogenase that consists of only the H-cluster catalytic domain, has been exploited for biochemical and spectroscopic studies.[25−31] The PetF [2Fe-2S] ferredoxin (Fd) has been shown to be the physiological electron donor for CrHydA1 during H_2-producing conditions in *C. reinhardtii*.[32,33] PetF donates electrons to CrHydA1 in a series of single-electron transfer steps, which makes CrHydA1 an ideal model system for investigating H-cluster intermediates and $2Fe_H$ subsite interactions that might be less accessible in mixed FeS cluster systems.[26,31] In this study, EPR and FTIR spectroscopy were applied to characterize CrHydA1 under steady-state oxidizing and reducing conditions in order to resolve further the electronic and vibrational properties of catalytic intermediates under turnover.

EXPERIMENTAL SECTION

Sample Preparation. CrHydA1 was heterologously expressed in *Escherichia coli* and purified as described previously.[34,35] Purification was carried out under strict anaerobic conditions in either a Coy chamber with a 3% H_2 (bulk N_2) atmosphere or an MBRAUN glovebox with a 100% N_2 atmosphere. In the final Strep-Tactin purification step, the enzyme was eluted in 50 mM Tris buffer (pH 8.0) containing 300 mM NaCl, 5% glycerol, and 5 mM sodium dithionite (NaDT). The purity of the enzyme was verified by sodium dodecyl sulfate polyacrylamide gel electrophoresis (SDS-PAGE), and the concentration was determined by Bradford assay. Typical yields were 3−5 mg/L of culture. The hydrogenase activity of CrHydA1 was determined by measuring H_2 evolution on a gas chromatograph (Agilent Technologies) after addition of 5 mM methyl viologen and 10 mM NaDT.

Auto-oxidized samples were prepared by incubation of CrHydA1 at 4 °C for 5−10 days in 50 mM Tris buffer (pH 8.0) containing 300 mM NaCl, 5% glycerol, and 5 mM NaDT in an MBRAUN glovebox (see Table 1 for a summary of sample conditions). Periodically, IR spectra of the samples were recorded, and when detectable changes in the spectra could no longer be observed, the samples were defined as auto-oxidized. For oxidation with thionin, the enzyme was passed over a G-25 column equilibrated in 50 mM Tris buffer (pH 8.0) containing 300 mM NaCl and 5% glycerol. Thionin (0.1 mM final concentration) was added to concentrated enzyme (0.5 mM) with stirring for 3 min. For samples treated with CO, CrHydA1 was flushed for 1 min with 100% CO gas and then incubated for 10 min under CO. For FTIR spectroscopy, auto-oxidized samples were treated with H_2 either by a 30 s flush with 100% H_2 followed by incubation for 15 min on ice or by 10 evacuation/flush cycles of samples in a sealed Wheaton conical vial with 100% H_2 on a Schlenk line equipped with an oxygen trap. For 100%-H_2-reduced EPR samples, a Wilmad pressure/vacuum EPR tube was evacuated and flushed with 100% H_2 for 10 cycles on the Schlenk line. For NaDT-reduced samples, CrHydA1 was incubated at room temperature for 1 min in 300 mM Tris buffer (pH 8.0) containing 300 mM NaCl, 5% glycerol, and a 10- or 20-fold molar excess of fresh NaDT relative to Fe content or overnight in a sealed vial at 4 °C in 2 or 10 mM NaDT. The concentrations of the prepared CrHydA1 samples ranged from 0.5 to 1 mM.

Table 1. Summary of CrHydA1 Sample Treatments

sample name	sample description
as-purified	isolated in buffer A[a] with 5 mM NaDT
auto-oxidized	as-purified enzyme incubated at 4 °C in buffer A with 5 mM NaDT until the IR spectra displayed no detectable changes (5−10 days)
100%-H_2-reduced	auto-oxidized enzyme subjected to 10 evacuation/flush cycles or flushing with 100% H_2
NaDT-reduced-1	auto-oxidized enzyme reduced with 2 mM NaDT overnight at 4 °C
NaDT-reduced-2	auto-oxidized enzyme reduced with a 10- or 20-fold molar excess of NaDT relative to Fe content at room temperature for 1 min
NaDT-reduced-3	auto-oxidized enzyme reduced with 10 mM NaDT overnight at 4 °C and then sequentially with a 10-fold molar excess of NaDT relative to Fe content at room temperature for 1 min

[a]Buffer A: 50 mM Tris (pH 8.0) containing 300 mM NaCl and 5% glycerol.

dx.doi.org/10.1021/ja4000257 | J. Am. Chem. Soc. XXXX, XXX, XXX−XXX

EPR Spectroscopy. Low-temperature EPR spectra of auto-oxidized and 100%-H_2-reduced samples were initially recorded on a Bruker EMX continuous-wave (CW) X-band spectrometer equipped with a liquid helium cryostat and temperature controller from Oxford Instruments and a 4102ST standard Bruker resonator. Later, low-temperature EPR spectra of NaDT-reduced and 100%-H_2-reduced samples were recorded on a Bruker ELEXSYS E500 CW X-band spectrometer equipped with a liquid helium cryostat and temperature controller from Oxford Instruments and an SHQ/0113 Bruker cavity. The magnetic field offset was determined with a 2,2-diphenyl-1-picrylhydrazyl (DPPH) standard from Bruker. Typical EPR parameters were as follows: sample temperature, 11 ± 1 K (10−65 K for temperature-dependence studies); microwave frequency, 9.37−9.38 GHz; microwave power, 1.0 mW (0.05−80 mW for power-dependence studies); time constant, 327.68 ms; modulation frequency, 100 kHz; modulation amplitude, 10.0 G.

Simulations of the experimental spectra were carried out using the EasySpin software package and used for determination of g values ($\pm 0.002g$) in some cases.[36] Spin quantifications were determined by double integration of the spectra and compared to spectra of copper standards under identical spectrometer conditions. Fractional contributions of individual simultions were calculated by double integration of the individual components that constituted the overall simulation.

FTIR Spectroscopy. FTIR spectra were collected with a Nicolet 6700 FTIR spectrometer (Thermo Fisher Scientific). The spectrometer was purged with N_2 gas passed through a glass desiccant tube filled with indicating Drierite and a miniature desiccant air dryer (Twin Tower Engineering) with pre- and post-desiccant filters. The spectrometer was equipped with a Globar IR source, a KBr beamsplitter, and a liquid-nitrogen-cooled mercury cadmium telluride (MCT) detector.

The sample cell consisted of a set of CaF_2 windows with a spacer and had a a path length of approximately 11 μm. The sample volume was approximately 5.5 μL. Spectra were created from raw data that consisted of 512 scans at 2 cm^{-1} resolution, collected by the OMNIC software program (Thermo Fisher Scientific). With a spectral resolution of 2 cm^{-1}, the data spacing was slightly less than 1 cm^{-1}, and a peak deviation of 1−2 cm^{-1} was considered as arising from the same vibrational mode. The reference spectrum was obtained using buffer solution, and the sample spectrum was recorded using buffer solution containing the enzyme sample. All of the spectra were collected at room temperature (21 °C). The OMNIC software was configured to report absorbance spectra, and absorbance baselines were fit to these data using a manually adjusted spline. Occasionally, spurious water absorption peaks due to slight changes in the water vapor concentration in the purge gas were seen. These water absorption peaks could be removed using a built-in atmospheric suppression algorithm in OMNIC.

RESULTS

EPR Spectroscopy. Heterologous expression and anaerobic purification of CrHydA1 yielded highly active enzyme, with typical hydrogenase activities of 739 ± 168 μmol H_2 min^{-1} mg^{-1}. The low-temperature X-band EPR spectrum of the as-purified enzyme displayed a sharp rhombic 2.1 signal (g = 2.100, 2.039, 1.997) along with a mixture of other signals (Figure 2a; see Table 2 for a summary of the EPR signals). After several days of incubation at 4 °C, the EPR spectrum was predominantly composed of a rhombic 2.1 signal [optimal temperature (T_{opt}) = 11 K] with smaller contributions from other signals (Figure 2b). A high-quality simulation could be obtained with contributions from g = 2.100, 2.039, 1.997 (96%) and g = 2.061, 1.968, 1.90 (4%) (Figure 2c). The rhombic 2.1 signal corresponds to the auto-oxidized enzyme and is in nice agreement with the rhombic 2.1 signal assigned to H_{ox} in previous reports.[11,14−16,25,31]

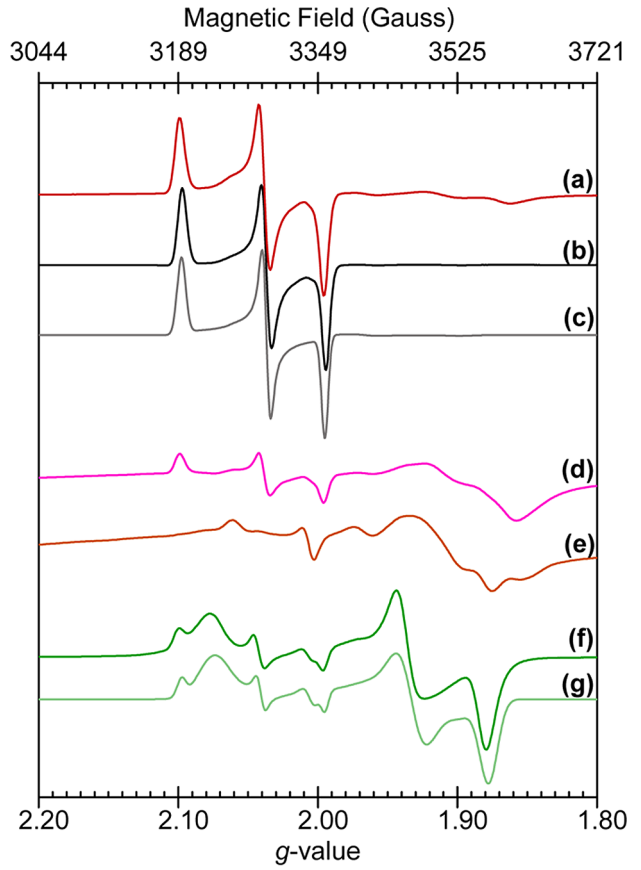

Figure 2. EPR spectra of CrHydA1 at 11 K under steady-state oxidizing and reducing conditions: (a) as-purified CrHydA1; (b) auto-oxidized CrHydA1; (c) simulation of auto-oxidized CrHydA1; (d) CrHydA1 after extensive evacuation/flushing under 100% H_2; (e) CrHydA1 NaDT-reduced-1; (f) CrHydA1 NaDT-reduced-2; (g) simulation of CrHydA1 NaDT-reduced-2. The experimental spectra were recorded at microwave power of 1.0 mW. Spectrometer settings: modulation frequency, 100 kHz; modulation amplitude, 10.0 G; time constant, 327.68 ms; microwave frequency, 9.37−9.38 GHz. Spectra were normalized to the sample concentration. A scaling factor of 4 was applied to (e) because of its overall lower intensity.

Oxidation of as-purified CrHydA1 with thionin (E_{m7} = +60 mV vs NHE), which has traditionally been used to oxidize [FeFe]-hydrogenase,[37] also yielded the rhombic 2.1 signal. However an additional axial feature at g = 2.007 was present and increased in intensity with longer thionin incubation time (Figure S1 in the Supporting Information). This feature is identical to part of the axial g = 2.05 signal that is formed upon CO inhibition of CrHydA1 (g = 2.045, 2.007, 2.007; Figure S1). The presence of g = 2.007 in the spectra of thionin-treated samples and other spectra reported herein may indicate that a fraction of the sample degrades and releases CO, which in turn is bound to other enzymes, creating the H_{ox}-CO signal. Similar observations have been reported in previous studies of DdH and CrHydA1.[16,19,25] To avoid these degradation artifacts, the as-purified auto-oxidized enzyme was used to characterize properties of the "H_{ox}" redox intermediate. The effects of thionin on CrHydA1 integrity were further explored by FTIR, and the results are summarized below.

The reduction of CrHydA1 by 100% H_2 resulted in a 68% attenuation of the rhombic 2.1 signal at 11 K relative to the initial H_{ox} signal, as determined by double spin integration (Figure 2d). The attenuation was correlated with the

dx.doi.org/10.1021/ja4000257 | J. Am. Chem. Soc. XXXX, XXX, XXX−XXX

Table 2. Summary of the EPR Signals Observed for CrHydA1

signal name	sample	g values	T_{opt} (K)[a]	reference figure(s)
rhombic 2.1	as-purified	2.100, 2.039, 1.997	11	2a
	auto-oxidized	2.100, 2.039, 1.997	11	2b
	100%-H_2-reduced	2.100, 2.043, 1.997	11	2d, 3
	NaDT-reduced-2,3	2.100, 2.043, 1.997	11	2f, 4, S3
broad 2.3−2.07	as-purified	1.867	11	2a
	100%-H_2-reduced	2.3−2.07,[b] 1.863 (1.876[c])	11	2d, 3, S2
	NaDT-reduced-1,3	2.3−2.07,[b] 1.863	11	2e, S3
rhombic 2.08	NaDT-reduced-2	2.077, 1.935, 1.880	10−15	2f, 4
	NaDT-reduced-3	2.078, 1.936, 1.880	10−15	S3
rhombic 2.06	as-purified	2.061, 1.968, 1.900	23	2a
	auto-oxidized	2.061, 1.968, 1.900	23	2b
	100%-H_2-reduced	2.061, 1.968, 1.900	23	2d, 3
	NaDT-reduced 1−3	2.061, 1.968, 1.900	23	2e,f, 4, S3
2.007	100%-H_2-reduced	2.007	23	2d, 3
	NaDT-reduced 1−3	2.007	23	2e,f, 4, S3
axial 2.05	CO	2.045, 2.007, 2.007	23	S1

[a]Optimal temperature. [b]Broad feature centered approximately between g = 2.3 and g = 2.07. [c]At 23 K.

appearance of a new heterogeneous signal consisting of a very broad feature centered approximately between g = 2.3 and g = 2.07 and a feature at g = 1.863 (the overall signal is herein termed the broad 2.3−2.07 signal). The fast-relaxing signal was most intense at 11 K and did not saturate easily with power (Figure 3 inset). Its intensity rapidly decreased as the temperature was raised to 23 K. Also, at 23 K, the feature at g = 1.863 shifted to g = 1.876 and did not saturate easily with power (Figure S2 in the Supporting Information). These properties are most consistent with those of [4Fe-4S] clusters,[38] suggesting that the source of this signal is an $S = {}^1/_2$ H-cluster containing a $[4Fe\text{-}4S]_H^+$ subcluster. Also present in the EPR spectrum of the 100%-H_2-reduced sample were a weak rhombic 2.06 signal (g = 2.061, 1.968, 1.900) and an axial feature at g = 2.007 (T_{opt} = 23 K). The rhombic 2.06 signal was most intense at 23 K and could be observed up to 50 K (Figure 3). This signal was also more susceptible to saturation with increasing power, similar to the rhombic 2.1 signal (Figure 3 inset). The temperature and power dependences of the rhombic 2.06 signal are most consistent with those of [2Fe-2S] clusters,[38] but assignment of this signal to a specific H-cluster intermediate remains challenging because it was present in a number of samples at varying quantities (see below).

Reduction of CrHydA1 by NaDT led to a variety of different EPR signals depending on the reaction conditions and incubation times. The different signals observed for NaDT reductions may reflect the heterogeneity of intermediate populations formed under turnover conditions. The NaDT-reduced-1 sample resulted in an EPR spectrum at 11 K similar to that of the 100%-H_2-reduced sample, and it displayed the g = 2.3−2.07 signal in addition to the rhombic 2.06 signal and the axial feature at g = 2.007 (Figure 2e). The NaDT-reduced-2 sample resulted in a complex EPR spectrum at 11 K, predominantly consisting of a new broad rhombic 2.08 signal (g = 2.077, 1.935, 1.880) (Figure 2f) with weaker contributions from the rhombic 2.1 signal (g = 2.100, 2.043, 1.997), the rhombic 2.06 signal, and the axial feature at g = 2.007. The NaDT-reduced-3 sample yielded a spectrum made up of a mixture of signals (Figure S3 in the Supporting Information). Overall, the rhombic 2.08 signal dominated the spectrum, with smaller contributions from the broad 2.3−2.07 signal, the rhombic 2.1 signal, the rhombic 2.06 signal, and the g = 2.007 axial feature.

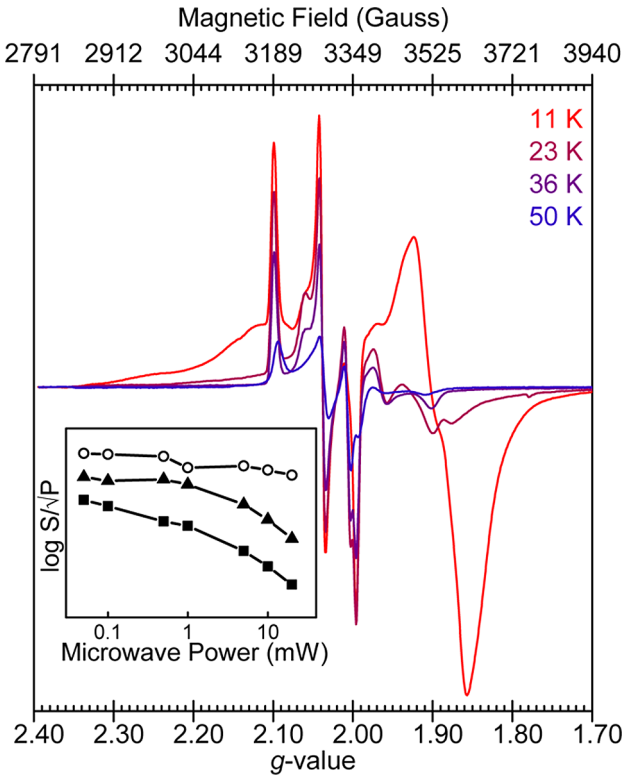

Figure 3. EPR temperature profile of 100%-H_2-reduced CrHydA1. Color scheme: gradient from red (11 K) to blue (50 K). The spectra were recorded at a microwave power of 1.0 mW and are presented as measured at temperatures of 11, 23, 36, and 50 K. The inset shows the microwave power dependence of the broad 2.3−2.07 (○), and rhombic 2.06 (▲) and 2.1 signals (■) as measured by the spectral features at g = 1.863, g = 2.06, and g = 2.10, respectively, at 11 K (S, signal amplitude; P, power). Other spectrometer settings were as described in the Figure 2 caption.

The power- and temperature-dependence properties of the rhombic 2.08 signal were also measured for the NaDT-reduced-2 sample. T_{opt} was determined to be between 10 and 15 K (Figure 4). As the temperature increased, the feature at g =

dx.doi.org/10.1021/ja4000257 | J. Am. Chem. Soc. XXXX, XXX, XXX−XXX

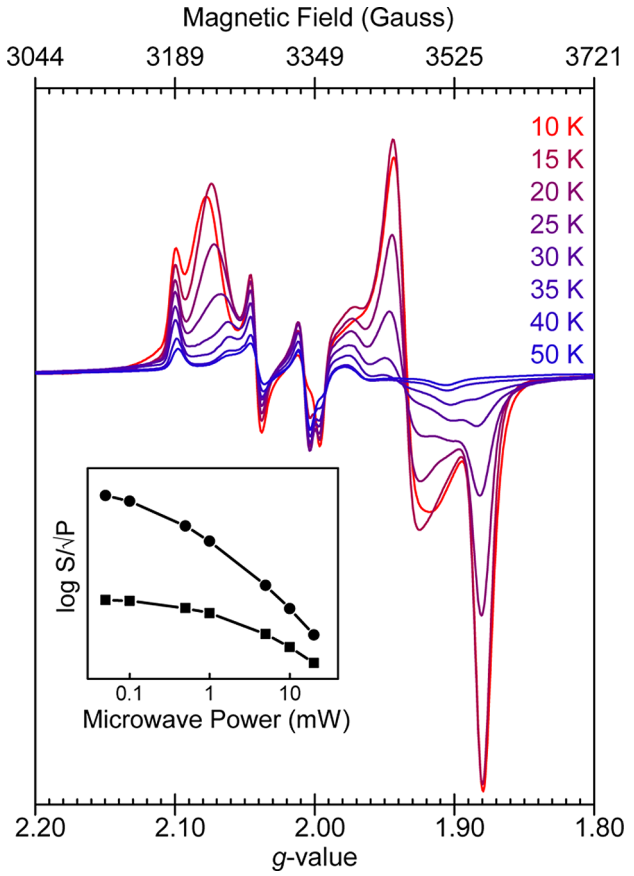

Figure 4. EPR temperature profile of the CrHydA1 NaDT-reduced-2 sample prepared with a 10-fold molar excess of NaDT relative to Fe content. Color scheme: gradient from red (10 K) to blue (50 K). The spectra were recorded at a microwave power of 1.0 mW and are presented as measured at temperatures 10, 15, 20, 25, 30, 35, 40, and 50 K. The inset shows the microwave power dependence of the rhombic 2.08 (●) and 2.1 (■) signals as measured by the spectral features at g = 2.077 and g = 2.10, respectively, at 11 K (S, signal amplitude; P, power). Other spectrometer settings were as described in the Figure 2 caption.

2.077 shifted to g = 2.072. Above 20 K, the signal broadened, and it was not visible above 30 K. At 11 K, the rhombic 2.08 signal saturated with power more quickly than the rhombic 2.1 signal (Figure 4 inset), but at 23 K, the signal did not saturate easily with power (Figure S4 in the Supporting Information). A high-quality simulation of the overall spectrum of the NaDT-reduced-2 sample at 11 K was obtained, and contributions from g = 2.100, 2.043, 1.997 (5%), g = 2.077, 1.935, 1.880 (90%), g = 2.065, 1.968, 1.900 (4%), and g = 2.045, 2.007, 2.007 (1%) were observed (Figure 2g). In these simulations, the broad peak at 2.077 was best reproduced using increased values of g strain, suggesting that the source of the signal may have increased spin−lattice relaxation and greater heterogeneity or anisotropy.

Overall, the temperature- and power-dependence properties of the rhombic 2.08 signal are most consistent with those of [4Fe-4S] clusters,[38] suggesting that the source of this signal, as for the broad 2.3−2.07 signal, is an $S = {}^1/_2$ H-cluster containing a $[4Fe\text{-}4S]_H^+$ subcluster. The g values of the observed rhombic 2.08 signal are comparable to those of other [4Fe-4S] cluster systems[39] and similar to the rhombic signal of "super-reduced" (H_{sred}) CrHydA1 reported earlier.[31] The possibility that it arises from the formation of an immature form of CrHydA1 containing only the $[4Fe\text{-}4S]_H^+$ subcluster is unlikely since the g values, the broad line shape, and the temperature- and power-dependence properties are different from those previously published for immature CrHydA1.[40,41] It is possible that the increased broadening and spin−lattice relaxation observed for the rhombic 2.08 signal, and even more so for the broad 2.3−2.07 signal observed after H_2 reduction, may arise from dipolar interactions or spin delocalization throughout the entire H-cluster due to electronic coupling between the $[4Fe\text{-}4S]_H^+$ subcluster and the $2Fe_H$ subsite via the cysteine thiolate ligand.[22,42−44]

FTIR Spectroscopy. To examine the structural properties of the $2Fe_H$ subsite in CrHydA1, FTIR spectroscopic analysis was performed in parallel with EPR on each of the samples. The IR spectrum in the 1775−2100 cm^{-1} region identifies the CO and CN ligand stretch modes of the $2Fe_H$ subsite, which are sensitive to redox changes in the H-cluster. As-purified CrHydA1 produced a spectrum consisting of a mixture of reduced and oxidized intermediates (Figure 5a; see Table 3 for

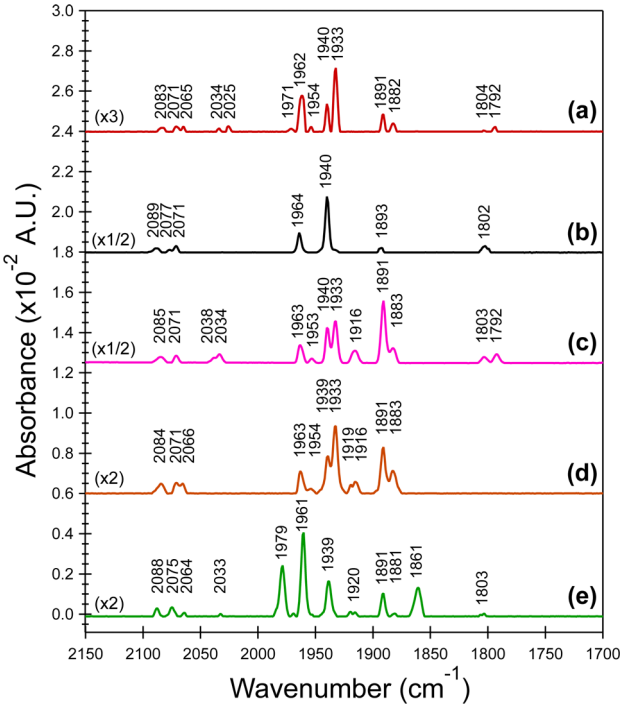

Figure 5. FTIR spectra of CrHydA1 under steady-state oxidizing and reducing conditions: (a) as-purified CrHydA1 (490 μM); (b) auto-oxidized CrHydA1 (510 μM); (c) CrHydA1 (820 μM) after extensive flushing under 100% H_2; (d) CrHydA1 (920 μM) NaDT-reduced-1; (e) CrHydA1 (820 μM) NaDT-reduced-2.

a summary of the FTIR peaks), consistent with the mixture of signals observed in the EPR spectrum. Auto-oxidized CrHydA1, which produced a uniform 2.1 H_{ox} EPR signal, showed a simplified FTIR spectrum composed predominately of five distinct peaks (Figure 5b), each of which could be assigned to one of the CO or CN ligand modes of $2Fe_H$. The dominant IR features are consistent with formation of H_{ox}[17−19,26] and include a bridging CO (CO_b) at 1802 cm^{-1}, a distal CO (CO_d) at 1940 cm^{-1}, and a proximal CO (CO_p) at 1964 cm^{-1} (distal and proximal refer to the position of the Fe atom of $2Fe_H$ relative to the $[4Fe\text{-}4S]_H$ subcluster). The CN modes were observed at 2071 and 2089 cm^{-1}. The low-intensity peak at

dx.doi.org/10.1021/ja4000257 | J. Am. Chem. Soc. XXXX, XXX, XXX−XXX

Table 3. Summary of the FTIR Absorbance Peaks Observed for CrHydA1

sample	CO and CN peaks (cm^{-1})[a]	reference figure
as-purified	1792, 1804, 1882, 1891, 1933, 1940, 1954, 1962, 1971, 2025, 2034, 2065, 2071, 2083	5a
auto-oxidized	1802, 1893, 1940, 1964, 2071, **2077**, 2089	5b
100%-H_2-reduced	1792, 1803, 1883, 1891, 1916, 1933, 1940, 1953, 1963, 2034, 2038, 2071, 2085	5c
NaDT-reduced-1	1883, 1891, 1916, 1919, 1933, 1939, 1954, 1963, **2066**, 2071, 2084	5d
NaDT-reduced-2	1803, **1861**, 1881, 1891, 1920, 1939, **1961**, **1979**, 2033, **2064**, **2075**, 2088	5e
NaDT-reduced-3	1885, 1891, 1939, **1961**, 1969, **1979**, 2051, 2082, 2086	S6

[a]Peaks in bold were not reported in previous studies of CrHydA1. The peak deviation value is 1−2 cm^{-1}, and peaks within this range are presumed to arise from the same vibrational mode.

1893 cm^{-1} indicates the presence of a small fraction of reduced H-clusters, which may account for the very weak rhombic 2.06 signal in the EPR spectrum.

Oxidation by treatment in thionin resulted in differential changes in the CO and CN region as a function of time that were not entirely consistent with the formation of H_{ox} (Figure S5 in the Supporting Information). When compared with the auto-oxidized sample, the thionin-treated sample showed the following features: (i) the appearance of peaks at 1968 and 2013 cm^{-1}, (ii) a shift of a CN peak to 2082 cm^{-1}, and (iii) a shift of CO_b from 1804 to 1808 cm^{-1}. All of these features were also observed after CO treatment of auto-oxidized CrHydA1 (H_{ox}-CO) (Figure S5). The feature at 2082 cm^{-1} is most likely composed of two or more overlapping peaks from both H_{ox} and H_{ox}-CO, on the basis of its broad shape. Together, the EPR and FTIR spectra of thionin-treated CrHydA1 suggest that the external oxidant leads to H-cluster degradation with concomitant formation of H_{ox}-CO by intact enzymes as described above. Except for the spectrum of thionin-oxidized CrHydA1, none of the FTIR spectra showed signs of CO inhibition/H-cluster degradation, whereas the EPR spectra showed indications of the presence of a small fraction of H_{ox}-CO by the presence of the g = 2.007 feature in both the 100%-H_2-reduced and NaDT-treated samples. It is likely that the amount of inhibited H-cluster was too small to be detectable by transmission FTIR spectroscopy, as low-temperature EPR spectroscopy is generally more sensitive to very low concentrations of species with strong paramagnetic centers.

Reduction of CrHydA1 by 100% H_2, which resulted in attenuation of the H_{ox} 2.1 EPR signal and the appearance of the broad 2.3−2.07 signal, caused a change from a simple FTIR spectrum (Figure 5b) to a more complex one (Figure 5c) (see Table 3). A difference spectrum for the 100%-H_2-reduced and auto-oxidized CrHydA1 samples (Figure 6a) showed new peaks (magenta trace) as positive absorptions at 1792, 1883, 1916, 1933, 1953, 2034, 2038, and 2085 cm^{-1} and an increase in the intensity at 1891/1893 cm^{-1}, whereas the peaks at 1802/1803, 1940, 1963/1964, 2071, and 2089 cm^{-1} that were present in the auto-oxidized sample all decreased in intensity. The peaks at 2034 and 2038 cm^{-1} are assigned as low-energy shifts in CN modes, as noted previously for DdH equilibrated at −420 mV.[19] The additional complexity of the CO region in the 100%-H_2-reduced sample indicates that the $2Fe_H$ subsite equilibrates to give a mixture of intermediates upon binding and activation of H_2. The majority of peaks observed for this

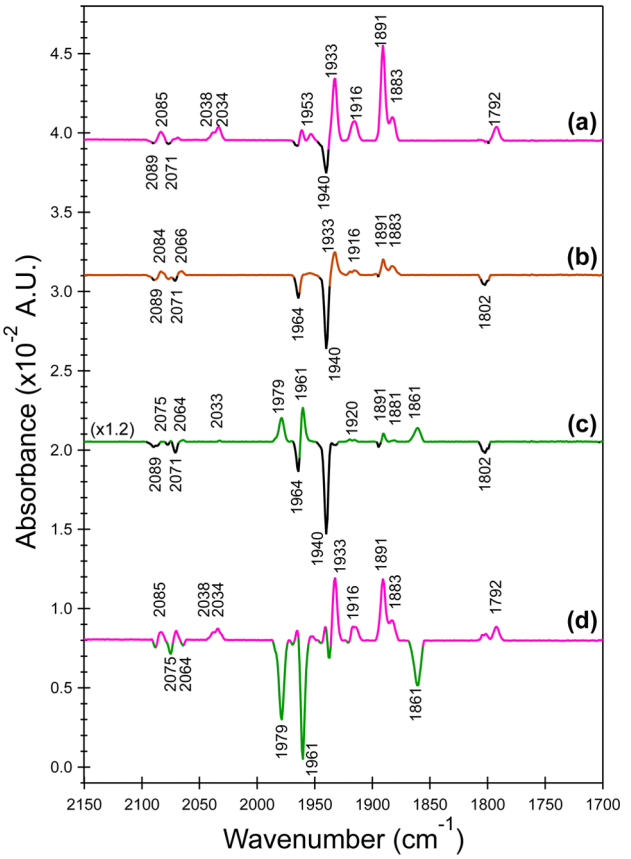

Figure 6. FTIR difference spectra contrasting the CrHydA1 samples shown in Figure 5: (a) 100%-H_2-reduced minus auto-oxidized; (b) NaDT-reduced-1 minus auto-oxidized; (c) NaDT-reduced-2 minus auto-oxidized; (d) 100%-H_2-reduced minus NaDT-reduced-2. A scaling factor of 4 was applied to the NaDT-reduced-2 spectrum prior to subtraction from the 100%-H_2-spectrum to zero out the 1939/1940 cm^{-1} peak and emphasize differences between the two samples. Color scheme: auto-oxidized, black; 100%-H_2-reduced, magenta; NaDT-reduced-1, orange; NaDT-reduced-2, green.

sample were previously assigned by spectroelectrochemical FTIR analysis of CrHydA1 as H_{red} (1793, 1891, 1935 cm^{-1}; E_m = −430 mV vs NHE, pH 8) or H_{sred} (1882, 1919, 1954 cm^{-1}; E_m = −510 mV vs NHE, pH 8) intermediates.[26] Each of these IR peaks was previously shown also to occur in CrHydA1 upon equilibration under 2% H_2, but with a lower intensity.[27]

Like the EPR spectra of the NaDT-treated CrHydA1 samples, different compositions of IR signals were observed for each set of reaction conditions and incubation times. The NaDT-reduced-1 sample (Figure 5d and Table 3) produced a spectrum similar to that obtained from H_2 reduction (Figure 5c). Presumably, consumption of the small amount NaDT from overnight incubation could create an overpressure of H_2 in the sealed vial, which may shift the H-cluster equilibrium toward intermediates that are common to ones formed through H_2 oxidation. The difference spectrum for the NaDT-reduced-1 and H_{ox} samples (Figure 6b, orange trace) showed positive absorptions at 1883, 1891, 1916, 1933, 2066, and 2084 cm^{-1}. Negative absorptions belonging to H_{ox} were observed at 1802, 1940, 1964, 2071, and 2089 cm^{-1}. Also, low-energy CO_b modes at 1792 and 1803 cm^{-1} that were present in the 100%-H_2-reduced sample were not observed for the NaDT-reduced-1 sample.

dx.doi.org/10.1021/ja4000257 | J. Am. Chem. Soc. XXXX, XXX, XXX−XXX

The NaDT-reduced-2 sample, which led to the appearance of a broad rhombic 2.08 EPR signal, caused the appearance of peaks at 1861, 1881, 1920, 1961, 1979, 2033, and 2064 cm^{-1} (Figure 5e and Table 3). A difference spectrum with respect to the auto-oxidized sample (Figure 6c, green trace) revealed unique features located throughout the CO and CN region. Positive absorptions at 1861, 1881, 1891, 1920, 1961, and 1979 cm^{-1} signify shifts in CO peaks that accompany redox and structural changes arising in the $2Fe_H$ subsite by addition of an electron from NaDT. The peaks at 2033 and 2064 cm^{-1} are assigned to the same low-energy shifts of CN modes as seen under treatment with 100% H_2. Thus, both the H_2 and NaDT reductions of CrHydA1 resulted in transitions from a homogeneous, predominantly H_{ox} spectrum into ones with greater complexity. The difference spectrum for the 100%-H_2-reduced and NaDT-reduced-2 samples (Figure 6d) highlights the distinct changes that occur at the $2Fe_H$ site with these two different treatments. Peaks at 1792, 1883, 1891, 1916, 1933, 2034, and 2038 cm^{-1} increased under 100% H_2 (magenta trace), whereas peaks at 1861, 1961, 1979 cm^{-1} were stronger after reduction with NaDT (green trace).

The NaDT-reduced-3 sample showed a spectrum displaying a mixture of absorption peaks (Figure S6 in the Supporting Information). While the spectrum more closely resembled that of the room-temperature NaDT-reduced-2 sample, it also showed peaks similar to those observed in the 100%-H_2-reduced sample. These included a stronger peak at 1891 cm^{-1} (relative to 1939 cm^{-1}) and a new peak at 1969 cm^{-1}. There was also an absence of peaks at 1803 cm^{-1} (assigned to CO_b of H_{ox}) and 1861 cm^{-1}.

DISCUSSION

The differential effects of treatment with H_2 versus NaDT were used to examine the reversibility of H-cluster intermediates formed during catalytic H_2 activation and H_2 evolution, respectively, in CrHydA1. Reduction of the H-cluster is possible by either the addition of electrons from natural (Fd) or chemical (NaDT) donors or by H_2 binding and oxidation in the presence of an electron acceptor. In the absence of an electron acceptor, H_2 binding and cleavage is a reversible process in CrHydA1. In contrast, the addition of NaDT resulted in catalytic turnover and H_2 production, as observed here during purification of CrHydA1 in NaDT buffers. Thus, the different reduction methods shift the steady-state equilibrium of the H-cluster to different populations of intermediates. For reductions by H_2, the g = 2.3−2.07 EPR signal was correlated with the appearance of FTIR peaks at 1883, 1891, 1916, and 1933 cm^{-1}. Overnight reduction by NaDT at 4 °C (i.e., NaDT-reduced-1) resulted in the appearance of the g = 2.3−2.07 EPR signal and FTIR peaks at 1883, 1891, 1916, and 1933 cm^{-1}, whereas addition of NaDT at room temperature (i.e., NaDT-reduced-2 and -3) predominantly led to the appearance of the rhombic 2.08 EPR signal and CO FTIR peaks at 1861, 1920, 1961, and 1979 cm^{-1}.

The appearance of a $[4Fe\text{-}4S]^+$ EPR signal under H_2 (g = 2.3−2.07) or NaDT (rhombic 2.08 and g = 2.3−2.07) demonstrates that other $S = {}^1/_2$ H-cluster intermediates, in addition to the rhombic 2.1 H_{ox} signal of the mixed-valent $2Fe_H$ subsite, occur during the catalytic cycle. There is precedent for the conversion of $[4Fe\text{-}4S]_H^{2+}$ to $[4Fe\text{-}4S]_H^{+}$ from the reductive activation of DdH purified in air. Upon treatment under H_2 or electrochemical reduction, a paramagnetic intermediate was formed at g = 2.06, 1.96, 1.89 that was later assigned as a $[4Fe\text{-}4S]_H^{+}$ species, but as a noncatalytic "H_{Trans}" form of the H-cluster.[13,14,16,23,24] The origin of that signal differs from the rhombic 2.08 and broad 2.3−2.07 signals observed here, which for CrHydA1 were formed under catalytic conditions. Accordingly, on the basis of the general model in Figure 1, we propose $[4Fe\text{-}4S]_H^{+}Fe(II)Fe(II)-H_2$, $[4Fe\text{-}4S]_H^{+}Fe(II)Fe(II)-H^-$, and $[4Fe\text{-}4S]_H^{+}Fe(I)Fe(I)-H^+$ as potential intermediates for the broad 2.3−2.07 and rhombic 2.08 signals (Figure 7), which share comparable EPR features

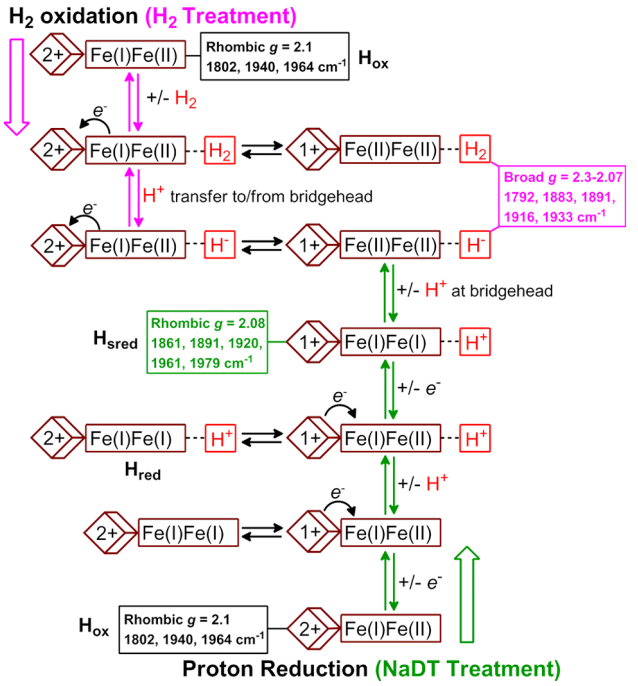

Figure 7. Hypothetical reaction diagram and proposed assignments of the H-cluster intermediates observed upon treatment of CrHydA1 with H_2 or NaDT (proton transfer to the bridgehead amine is not pictured). The EPR and prominent FTIR spectroscopic signals (CO peaks) observed in this study are indicated in the boxes, along with the previously assigned states[10,26,31] (i.e., H_{ox}, H_{red}, and H_{sred}). The cubes represent the $[4Fe\text{-}4S]_H$ subcluster, while FeFe represents the $2Fe_H$ subsite. Electron transfer between the two subsites is indicated by the curved arrows ($Fe_{proximal}$ and Fe_{distal} of the $2Fe_H$ subsite are not specified).

under certain conditions. While this agrees with previous FTIR and EPR characterization studies that first identified the H_{sred} state in CrHydA1[26,31] and assigned it as a $[4Fe\text{-}4S]_H^{+}Fe(I)$-$Fe(I)-H^+$ intermediate, our results further suggest that additional H-cluster intermediates with a 1+ cubane subsite are formed during catalysis. Mechanistically, Figure 7 suggests more complexity than indicated by the general model in Figure 1 and the model proposed by Adamska et al.[31] This is illustrated by the number of absorption features in the IR spectra of the reduced samples. Furthermore, it highlights that the two reductive processes converge upon common intermediates and suggests that certain reduced intermediates can be enriched in CrHydA1.

The presence of F-clusters in [FeFe]-hydrogenases such as CpI, DdH, and DvH helps clarify why the new catalytically relevant intermediates observed here were not detected in previous studies of these enzymes. By functioning to shuttle electrons in and out of the H-cluster as rapidly as possible to

dx.doi.org/10.1021/ja4000257 | J. Am. Chem. Soc. XXXX, XXX, XXX−XXX

facilitate high turnover rates, F-clusters make it difficult to trap catalytic intermediates containing $[4Fe\text{-}4S]_H^+$ subclusters. It is expected that $[4Fe\text{-}4S]_H^+$ can oxidize quickly to $[4Fe\text{-}4S]_H^{2+}$ as electrons are exchanged with F-clusters,[31] where they may be, in essence, stored. Conversely, in CrHydA1, the absence of F-clusters makes it possible to shift the equilibrium toward reduced $[4Fe\text{-}4S]_H^+$ intermediates,[31] as there are no possible outlets for electron flow besides the $2Fe_H$ subsite. Consequently, reduced H-cluster intermediates are more accessible to characterization in CrHydA1. Also, reduced F-clusters give rise to strong, broad EPR signals that could overshadow other underlying signals from reduced catalytic intermediates, preventing definitive assignments. For example, NaDT- and H_2-reduced CpI and DdH exhibited broad EPR spectra that covered the approximate range of the rhombic 2.08 signal and the broad 2.3−2.07 signal observed here for NaDT- and H_2-reduced CrHydA1.[11,13−16,45−47] Likewise, for CpII, another mixed FeS [FeFe]-hydrogenase, multiple signals were observed upon reduction with H_2 in the presence of NaDT, including an underlying very broad signal at low temperature that was assigned to a rapidly relaxing species.[11]

CONCLUSIONS

We have characterized the occurrence and properties of novel EPR and FTIR signals in the reduced H-cluster and assigned them to intermediates of catalytic turnover. Our results indicate that the H-cluster mechanism in CrHydA1, and therefore the catalytic cycle of [FeFe]-hydrogenases in general, involves formal reduction of the $[4Fe\text{-}4S]_H$ subcluster from the 2+ state to the 1+ state. This is similar to a previous model put forth by Adamska et al.[31] involving an H_{sred} intermediate. However, our results suggest that several $S = {}^1/_2$ H-cluster intermediates occur in CrHydA1 during catalysis, and two $[4Fe\text{-}4S]_H^+$ subcluster signals were identified during the proton reduction and H_2 oxidation cycles (see Figures 2 and 7). The complete activation/oxidation of H_2 is a coupled two-electron/two-proton reaction, and it is possible that a $[4Fe\text{-}4S]_H^+$ subcluster would form twice during each successive turnover event, consistent with the complexity of the EPR and FTIR signals in reduced enzymes. The model agrees with evidence for redox coupling between the two subsites in H-cluster models,[22,48,49] which has been proposed to function in facilitating milder reaction potentials during catalysis. Density functional theory studies of [FeFe]-hydrogenases[50] have also shown viable mechanistic pathways for inclusion of the $[4Fe\text{-}4S]_H^+$ subcluster in H_2 activation. In CrHydA1, the $[4Fe\text{-}4S]_H$ subcluster exchanges reducing equivalents with either the $2Fe_H$ subsite or external acceptors such as Fd. In this regard, we and others[31] speculate that in addition to the functions mentioned above, a transition in the $[4Fe\text{-}4S]_H$ subcluster between the 2+ and 1+ oxidation states would accommodate the electron transfer steps with Fd that are required to complete turnover during proton reduction or H_2 activation.

ASSOCIATED CONTENT

Supporting Information

Additional EPR and FTIR spectra of CO- and thionin-treated CrHydA1, EPR and FTIR spectra of NaDT-reduced CrHydA1, and microwave power dependence of the EPR spectra of 100%-H_2-reduced and NaDT-reduced CrHydA1 at 23 K. This material is available free of charge via the Internet at http://pubs.acs.org.

AUTHOR INFORMATION

Corresponding Author

paul.king@nrel.gov

Notes

The authors declare no competing financial interest.

ACKNOWLEDGMENTS

D.W.M., M.W.R., S.M.N., and P.W.K. gratefully acknowledge funding by the U.S. Department of Energy, Division of Chemical Sciences, Geosciences, and Biosciences, Office of Basic Energy Sciences, for the preparation of hydrogenases and FTIR and EPR spectroscopy and support by the U.S. Department of Energy under Contract DE-AC36-08-GO28308 with the National Renewable Energy Laboratory. E.M.S., A.S.B., J.W.P., and J.B.B. gratefully acknowledge funding by the U.S. Department of Energy, Division of Chemical Sciences, Geosciences, and Biosciences, Office of Basic Energy Sciences, through Grant DE-FG02-10ER16194. The authors thank Sandra and Gareth Eaton (University of Denver) for helpful discussions on EPR spectroscopy, Morgan Bye (University of East Anglia) for making available his EPR toolbox software package for data processing, David Bobela and Calvin Curtis (NREL) for technical assistance on the EPR system, and Marko Boehm (NREL) for generously providing TEV protease samples.

REFERENCES

(1) Vignais, P. M.; Billoud, B. *Chem. Rev.* **2007**, *107*, 4206.
(2) Ghirardi, M. L.; Dubini, A.; Yu, J.; Maness, P. C. *Chem. Soc. Rev.* **2009**, *38*, 52.
(3) Peters, J. W.; Lanzilotta, W. N.; Lemon, B. J.; Seefeldt, L. C. *Science* **1998**, *282*, 1853.
(4) Nicolet, Y.; Piras, C.; Legrand, P.; Hatchikian, C. E.; Fontecilla-Camps, J. C. *Structure* **1999**, *7*, 13.
(5) Silakov, A.; Wenk, B.; Reijerse, E.; Lubitz, W. *Phys. Chem. Chem. Phys.* **2009**, *11*, 6592.
(6) van der Spek, T. M.; Arendsen, A. F.; Happe, R. P.; Yun, S.; Bagley, K. A.; Stufkens, D. J.; Hagen, W. R.; Albracht, S. P. *Eur. J. Biochem.* **1996**, *237*, 629.
(7) Pierik, A. J.; Hulstein, M.; Hagen, W. R.; Albracht, S. P. *Eur. J. Biochem.* **1998**, *258*, 572.
(8) Kubas, G. J. *Chem. Rev.* **2007**, *107*, 4152.
(9) Bruschi, M.; Greco, C.; Bertini, L.; Fantucci, P.; Ryde, U.; Gioia, L. D. *J. Am. Chem. Soc.* **2010**, *132*, 4992.
(10) Lubitz, W.; Reijerse, E.; van Gastel, M. *Chem. Rev.* **2007**, *107*, 4331.
(11) Adams, M. W. W. *J. Biol. Chem.* **1987**, *262*, 15054.
(12) Johnson, M. K.; Morningstar, J. E.; Oliver, M.; Frerman, F. E. *FEBS Lett.* **1987**, *226*, 129.
(13) Patil, D. S.; Moura, J. J. G.; He, S. H.; Teixeira, M.; Prickril, B. C.; Dervartanian, D. V.; Peck, H. D.; Legall, J.; Huynh, B. H. *J. Biol. Chem.* **1988**, *263*, 18732.
(14) Pierik, A. J.; Hagen, W. R.; Redeker, J. S.; Wolbert, R. B.; Boersma, M.; Verhagen, M. F.; Grande, H. J.; Veeger, C.; Mutsaers, P. H.; Sands, R. H.; Dunham, W. R. *Eur. J. Biochem.* **1992**, *209*, 63.
(15) Bennett, B.; Lemon, B. J.; Peters, J. W. *Biochemistry* **2000**, *39*, 7455.
(16) Albracht, S. P. J.; Roseboom, W.; Hatchikian, E. C. *J. Biol. Inorg. Chem.* **2006**, *11*, 88.
(17) Nicolet, Y.; Ade Lacey, A. L.; Vernede, X.; Fernandez, V. M.; Hatchikian, E. C.; Fontecilla-Camps, J. C. *J. Am. Chem. Soc.* **2001**, *123*, 1596.
(18) Chen, Z.; Lemon, B. J.; Huang, S.; Swartz, D. J.; Peters, J. W.; Bagley, K. A. *Biochemistry* **2002**, *41*, 2036.
(19) Roseboom, W.; De Lacey, A. L.; Fernandez, V. M.; Hatchikian, E. C.; Albracht, S. P. J. *J. Biol. Inorg. Chem.* **2006**, *11*, 102.

(20) Carroll, M. E.; Barton, B. E.; Rauchfuss, T. B.; Carroll, P. J. *J. Am. Chem. Soc.* **2012**, *134*, 18843.
(21) Zaffaroni, R.; Rauchfuss, T. B.; Gray, D. L.; De Gioia, L.; Zampella, G. *J. Am. Chem. Soc.* **2012**, *134*, 19260.
(22) Tard, C.; Liu, X.; Ibrahim, S. K.; Bruschi, M.; Gioia, L. D.; Davies, S. C.; Yang, X.; Wang, L.-S.; Sawers, G.; Pickett, C. J. *Nature* **2005**, *433*, 610.
(23) Popescu, C. V.; Münck, E. *J. Am. Chem. Soc.* **1999**, *121*, 7877.
(24) Pereira, A. S.; Tavares, P.; Moura, I.; Moura, J. J. G.; Huynh, B. H. *J. Am. Chem. Soc.* **2001**, *123*, 2771.
(25) Kamp, C.; Silakov, A.; Winkler, M.; Reijerse, E. J.; Lubitz, W.; Happe, T. *Biochim. Biophys. Acta* **2008**, *1777*, 410.
(26) Silakov, A.; Kamp, C.; Reijerse, E.; Happe, T.; Lubitz, W. *Biochemistry* **2009**, *48*, 7780.
(27) Kuchenreuther, J. M.; Grady-Smith, C. S.; Bingham, A. S.; George, S. J.; Cramer, S. P.; Swartz, J. R. *PLoS One* **2010**, *5*, No. e15491.
(28) Cornish, A. J.; Gartner, K.; Yang, H.; Peters, J. W.; Hegg, E. L. *J. Biol. Chem.* **2011**, *286*, 38341.
(29) Knorzer, P.; Silakov, A.; Foster, C. E.; Armstrong, F. A.; Lubitz, W.; Happe, T. *J. Biol. Chem.* **2012**, *287*, 1489.
(30) Morra, S.; Giraudo, A.; Di Nardo, G.; King, P. W.; Gilardi, G.; Valetti, F. *PLoS One* **2012**, *7*, No. e48400.
(31) Adamska, A.; Silakov, A.; Lambertz, C.; Rudiger, O.; Happe, T.; Reijerse, E.; Lubitz, W. *Angew. Chem., Int. Ed.* **2012**, *51*, 11458.
(32) Melis, A.; Happe, T. *Plant Physiol.* **2001**, *127*, 740.
(33) Florin, L.; Tsokoglou, A.; Happe, T. *J. Biol. Chem.* **2001**, *276*, 6125.
(34) King, P. W.; Posewitz, M. C.; Ghirardi, M. L.; Seibert, M. *J. Bacteriol.* **2006**, *188*, 2163.
(35) Yacoby, I.; Tegler, L. T.; Pochekailov, S.; Zhang, S.; King, P. W. *PLoS One* **2012**, *7*, No. e35886.
(36) Stoll, S.; Schweiger, A. *J. Magn. Reson.* **2006**, *178*, 42.
(37) Adams, M. W.; Johnson, M. K.; Zambrano, I. C.; Mortenson, L. E. *Biochimie* **1986**, *68*, 35.
(38) Rupp, H.; Rao, K. K.; Hall, D. O.; Cammack, R. *Biochim. Biophys. Acta* **1978**, *537*, 255.
(39) Guigliarelli, B.; Bertrand, P. *Adv. Inorg. Chem.* **1999**, *47*, 421.
(40) Mulder, D. W.; Ortillo, D. O.; Gardenghi, D. J.; Naumov, A. V.; Ruebush, S. S.; Szilagyi, R. K.; Huynh, B.; Broderick, J. B.; Peters, J. W. *Biochemistry* **2009**, *48*, 6240.
(41) Czech, I.; Silakov, A.; Lubitz, W.; Happe, T. *FEBS Lett.* **2010**, *584*, 638.
(42) Fiedler, A. T.; Brunold, T. C. *Inorg. Chem.* **2005**, *44*, 9322.
(43) Schwab, D. E.; Tard, C.; Brecht, E.; Peters, J. W.; Pickett, C. J.; Szilagyi, R. K. *Chem. Commun.* **2006**, 3696.
(44) Giles, L. J.; Grigoropoulos, A.; Szilagyi, R. K. *Eur. J. Inorg. Chem.* **2011**, 2677.
(45) Erbes, D. L.; Burris, R. H.; Orme-Johnson, W. H. *Proc. Natl. Acad. Sci. U.S.A.* **1975**, *72*, 4795.
(46) Grande, H. J.; Dunham, W. R.; Averill, B.; Van Dijk, C.; Sands, R. H. *Eur. J. Biochem.* **1983**, *136*, 201.
(47) Zambrano, I. C.; Kowal, A. T.; Mortenson, L. E.; Adams, M. W.; Johnson, M. K. *J. Biol. Chem.* **1989**, *264*, 20974.
(48) Tard, C.; Pickett, C. J. *Chem. Rev.* **2009**, *109*, 2245.
(49) Camara, J. M.; Rauchfuss, T. B. *Nat. Chem.* **2012**, *4*, 26.
(50) Greco, C.; Bruschi, M.; Fantucci, P.; Ryde, U.; De Gioia, L. *J. Am. Chem. Soc.* **2011**, *133*, 18742.